Journal of Applied Physics

RESEARCH ARTICLE | FEBRUARY 13 2026

Performance enhancement of AlGaN/GaN-based high electron mobility transistors with sputtered AlScN gate dielectric

A. Yassine ; R. Driad ; A. Nair ; P. Ott ; L. Kirste ; P. Straňák ; H. Czap ; M. Mikulla ; M. Yassine ; O. Ambacher

J. Appl. Phys. 139, 064503 (2026)
https://doi.org/10.1063/5.0301760

Articles You May Be Interested In

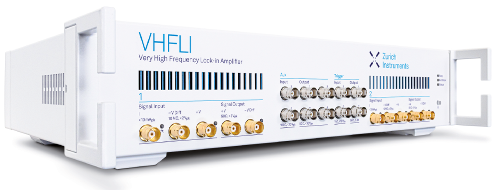

AIP Publishing

Journal of Applied Physics ARTICLE pubs.aip.org/aip/jap

Performance enhancement of AlGaN/GaN-based high electron mobility transistors with sputtered AlScN gate dielectric

Cite as: J. Appl. Phys. **139**, 064503 (2026); doi: 10.1063/5.0301760
Submitted: 10 September 2025 · Accepted: 9 January 2026 ·
Published Online: 13 February 2026

View Online Export Citation CrossMark

A. Yassine,[1,a)] R. Driad,[2] A. Nair,[2] P. Ott,[1] L. Kirste,[2] P. Straňák,[2] H. Czap,[2] M. Mikulla,[2] M. Yassine,[1] and O. Ambacher[1]

AFFILIATIONS

[1]Institute for Sustainable Systems Engineering INATECH, Albert-Ludwigs-University Freiburg, Emmy-Noether-Str. 2, Freiburg D-79110, Germany
[2]Fraunhofer Institute for Applied Solid State Physics IAF, Tullastr. 72, Freiburg D-79108, Germany

[a)]**Author to whom correspondence should be addressed:** ali.yassine@inatech.uni-freiburg.de

ABSTRACT

This study explores the effects of a sputtered $Al_{0.7}Sc_{0.3}N$ layer deposited onto metalorganic chemical vapor deposition-grown $Al_{0.3}Ga_{0.7}N$/GaN heterostructures, with a focus on structural and electrical properties, including DC characteristics of high-electron-mobility transistors (HEMTs). Structural analysis reveals that a 25 nm AlScN layer preserves surface roughness and barrier/channel interface quality, although relaxation occurs due to non-ideal growth conditions. Capacitance–voltage profiling indicates a sharp and uniform depletion, with reduced hysteresis post-deposition, suggesting effective passivation. Incorporation of AlScN increases the sheet carrier density from 1.4 to 1.89×10^{13} cm^{-2}, although this is accompanied by lower mobility and a modest rise in sheet resistance from 406 to 441 Ω/sq. Devices with a 0.7 μm gate length demonstrate a saturation current of 0.98 A/mm, approximately 30% higher than reference AlGaN/GaN HEMTs. The composite barrier configuration further exhibits reduced leakage and improved insulation, but results in decreased transconductance and a pronounced threshold voltage shift from −0.8 to −7.8 V, attributed to increased barrier thickness. On-resistance also rises from 2 to 2.5 Ω mm likely due to sputter-induced contact damage. Optimization with a thinner 15 nm AlScN layer achieves a favorable balance, enhancing saturation current and soft-breakdown voltage while minimizing drawbacks in transconductance and on-resistance. Overall, sputtered AlScN serves as both a high-quality barrier and passivation layer, yielding enhanced device performance and robustness, and highlighting the future potential of sputter epitaxy to further advance GaN technology.

I. INTRODUCTION

AlScN has attracted considerable attention in recent years as a barrier material for GaN-based high-electron-mobility transistors (HEMTs).[1,2] Its tunable lattice constant allows near-lattice matching to GaN at moderate scandium concentrations[3–5] while retaining the high spontaneous polarization of AlN[6,7] and exhibiting an enhanced piezoelectric response.[8] This combination enables the formation of a two-dimensional electron gas (2DEG) with sheet carrier densities and consequently transistor current densities significantly higher than those achievable with conventional AlGaN barriers.[9–11] Consequently, AlScN holds strong potential for advancing high-frequency and high-power GaN-based electronics.

The successful integration of AlScN into GaN heterostructures and the device performance, however, critically depend on the choice of epitaxial growth technique. Molecular beam epitaxy (MBE) was the first method used to realize AlScN/GaN HEMTs.[12] It demonstrated the material's potential, with high sheet carrier densities above 3×10^{13} cm^{-2}[12–14] and current densities exceeding 3 A/mm.[13,14] Yet, MBE is fundamentally limited in throughput and scalability, which restricts its suitability for mass production.

Metalorganic chemical vapor deposition (MOCVD) offers a more industrially viable path, combining high material quality with scalability. Several works have successfully demonstrated MOCVD-grown AlScN/GaN heterostructures with sheet resistances lower than 250 Ω/sq[15–17] and devices achieving current densities above 1.7 A/mm.[18,19] Despite these encouraging results, the MOCVD growth of AlScN remains challenging due to high growth temperatures, slow growth rates, and impurity incorporation from scandium precursors.[15–17] These factors promote interfacial diffusion[17,20] and introduce carbon and oxygen impurities that degrade carrier concentration[17,20,21] and electron mobility[17,20] and limit device breakdown performance.[22] Similar impurity-related issues have also been observed in MBE-grown AlScN layers, showing a strong dependence on elemental Sc source purity.[23,24] Studies by Casamento *et al.*[25] and Nomoto *et al.*[14] further revealed carrier freeze-out effects and breakdown fields well below the intrinsic material limits, respectively, underscoring the persistent challenges.

Sputter epitaxy offers an alternative means of growing AlScN, with advantages in cost, scalability, and reduced processing temperatures compared to MBE and MOCVD.[26] Although sputtered wurtzite AlScN is more established than growth via other methods,[27] achieving the crystalline quality and interface sharpness required for HEMTs remains a challenge, such that the direct formation of 2DEGs by sputtered AlScN on GaN has yet not been realized, despite notable progress.[28,29] Recent studies, however, have highlighted its potential when combined with MOCVD-grown heterostructures.[30,31] Okuda *et al.*[30] demonstrated that sputtering an AlScN layer with 6% Sc concentration onto AlGaN/GaN HEMTs enhanced the 2DEG density, indicating the potential of sputtered epitaxy to improve the conventional GaN technology. This result was further supported by Ota *et al.*,[31] who observed nearly a threefold increase in the sheet carrier density after AlScN regrowth on AlGaN/GaN compared to the reference structure. Despite these advances, improvements have not yet been conclusively demonstrated at the transistor level. While Maeda *et al.*[32] have recently reported the first AlGaN/GaN transistors incorporating a sputtered $Al_{0.91}Sc_{0.09}N$ layer, a direct comparison with reference AlGaN/GaN HEMTs to confirm these benefits is still lacking.

This work aims to advance the understanding of AlScN integration in GaN-based electronics by investigating the regrowth of AlScN layers with 30% Sc concentration on MOCVD-grown $Al_{0.3}Ga_{0.7}N$/GaN heterostructures. The study systematically evaluates both the structural and electrical properties of the regrown layers and extends the analysis to the DC performance of HEMTs featuring AlScN/AlGaN composite barriers with a sputtered AlScN gate dielectric. A direct comparison with reference AlGaN/GaN devices is undertaken, with particular focus on transfer and output characteristics as well as off-state behavior. By assessing the role of AlScN thickness, this work provides a comprehensive demonstration of the potential of sputtered AlScN at the transistor level and highlights its prospects for enabling next-generation high-frequency and high-power GaN devices.

II. GROWTH AND CHARACTERIZATION OF AlScN/AlGaN/GaN HETEROSTRUCTURES

The epitaxial growth of AlGaN/GaN heterostructures was performed using a multiwafer metalorganic chemical vapor deposition (MOCVD) system. Trimethylgallium (TMGa), trimethylaluminum (TMAl), and ammonia (NH_3) served as the gallium, aluminum, and nitrogen precursors, respectively, with hydrogen (H_2) employed as the carrier gas throughout the deposition process. All layers were deposited on 4 in. sapphire substrates. The epitaxial stack consisted of an approximately 1 μm thick Fe-compensated GaN buffer layer, followed by a 1 μm unintentionally doped GaN channel layer. For the reference heterostructure, a 13 nm $Al_{0.3}Ga_{0.7}N$ barrier layer was subsequently grown and capped with a 2 nm GaN layer.

The AlScN dielectric layer was deposited by reactive pulsed DC magnetron co-sputtering using an Evatec Radiance Cluster Sputter Tool. Deposition was carried out directly on the previously described AlGaN/GaN heterostructure stack. A mixed nitrogen (N_2) and argon (Ar) atmosphere ($N_2/(Ar + N_2) \sim 71.5\%$) was used as the process gas, with the growth conducted at a temperature of 400 °C, which was chosen based on the growth optimization of AlScN layers on sapphire substrates, as reported in a previous study,[33] and a process pressure of 9.5×10^{-4} mbar. The sputtering powers for the aluminum and scandium targets were set to 1000 and 670 W, respectively, with a target-to-substrate distance of 65 mm. Under these conditions, the deposition produced an AlScN film with a thickness of 25 nm, as determined by x-ray reflectometry (XRR) and high-resolution x-ray diffraction (HRXRD). Time-of-flight secondary ion mass spectrometry (ToF-SIMS) analysis further confirmed a scandium concentration of 30% in the film. An AlScN layer with 30% Sc concentration was targeted to reproduce the barrier structures proposed by Wang *et al.*[34]

To characterize the surface morphology and roughness, atomic force microscopy (AFM) in the tapping mode was performed, with roughness quantified as the root-mean-square average. Figure 1 shows the AFM images of the surface of the AlGaN/GaN heterostructures without and with AlScN layer on top. The AlGaN/GaN reference structure exhibits a root mean square (rms) of 0.53 nm, indicating a uniform and a homogeneous surface morphology. The rms increased to 0.71 nm after the deposition of the AlScN layer on top. The heterostructure with an AlScN dielectric layer exhibits slightly larger height variations evident by the increased color scale, but maintains a similar overall texture. However, the preservation of the terrace steps and low roughness value after AlScN deposition points to limited surface damage during sputtering.

For further structural analysis, HRXRD measurements were performed using a PANalytical X'Pert Pro MRD diffractometer. The θ/2θ scans and rocking curve (ω-scans) of the 0002 reflection were recorded at the center of each wafer. To assess the crystalline quality and investigate the epitaxial relation between the AlScN and the underlying AlGaN/GaN layers, reciprocal space mapping (RSM) was performed. The results are presented in Fig. 2.

Prior to AlScN deposition, clear thickness fringes are observed in addition to the pronounced diffraction peaks corresponding to the AlGaN and GaN layers, indicating well-defined and abrupt interfaces within the heterostructure [see Fig. 2(a)]. After sputtering, a distinct diffraction peak corresponding to the AlScN layer becomes visible, accompanied by thickness fringes. The continued presence of these fringes suggests that the interface quality and abruptness remain largely unaffected upon AlScN deposition. The sharpness of the AlScN diffraction peak reflects the high crystalline quality of the layer and suggests minimal formation of secondary phases. This observation is further supported by rocking curve measurements [Fig. 2(b)], which demonstrate a narrow full width

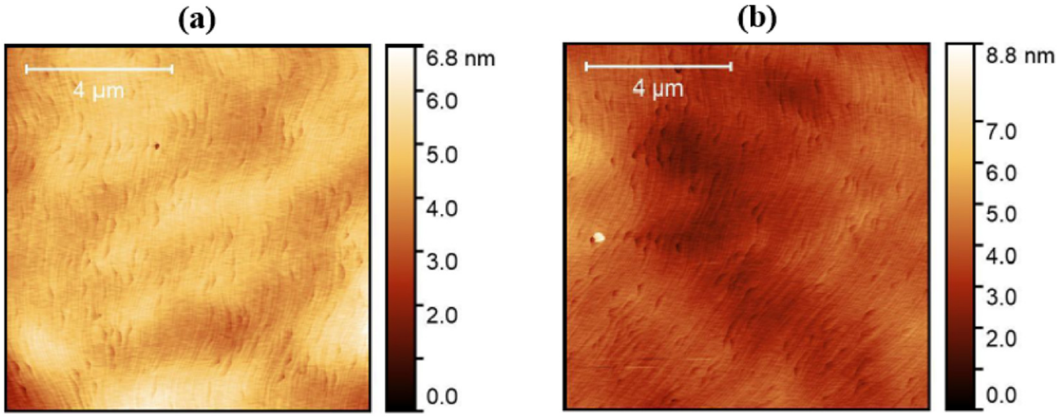

FIG. 1. AFM images of the surface of the $Al_{0.3}Ga_{0.7}N$/GaN HEMT structure before (a) and after (b) deposition of a 25 nm AlScN layer on top.

at half maximum (FWHM) of 0.09°. Reciprocal space mapping analysis [Fig. 2(c)] indicates the relaxation of the AlScN layer, as evidenced by the misalignment of the q_x coordinate of the AlScN plane relative to that of the GaN layer. The lattice parameters *c* and *a* of the AlScN layer were determined to be 5.04 and 3.25 Å, respectively, corresponding to an in-plane lattice mismatch of approximately 2% with respect to the underlying GaN layer.

At first glance, this relaxation appears to be due to the AlScN layer exceeding the critical thickness for pseudomorphic growth.[3] However, several studies emphasize a significant dependence of the lattice parameters not only on the growth techniques,[35] but also on the growth temperatures.[31,35,36] For instance, Kobayashi *et al.*[28] demonstrated the coherent growth of AlScN on GaN by sputter epitaxy at comparable Sc concentration and even higher thicknesses but at different growth temperatures than those used here. Collectively, these observations suggest that the current growth parameters are suboptimal, and further process optimization is required to improve film quality and minimize relaxation effects.

ToF-SIMS was employed to further assess the compositional uniformity of the fabricated layers and to probe the quality of the interfaces, as depicted in Fig. 3. A homogenous AlGaN barrier is observed, as evidenced by the stable Al and Ga signals throughout the barrier region. Furthermore, a well-defined transition is observed at the AlGaN/GaN interface, as indicated by the abrupt increase in the Ga signal and sharp decrease in the Al signal, suggesting a chemically abrupt interface.

Notably, the AlScN dielectric layer also demonstrates a uniform composition, despite its relatively limited thickness. This

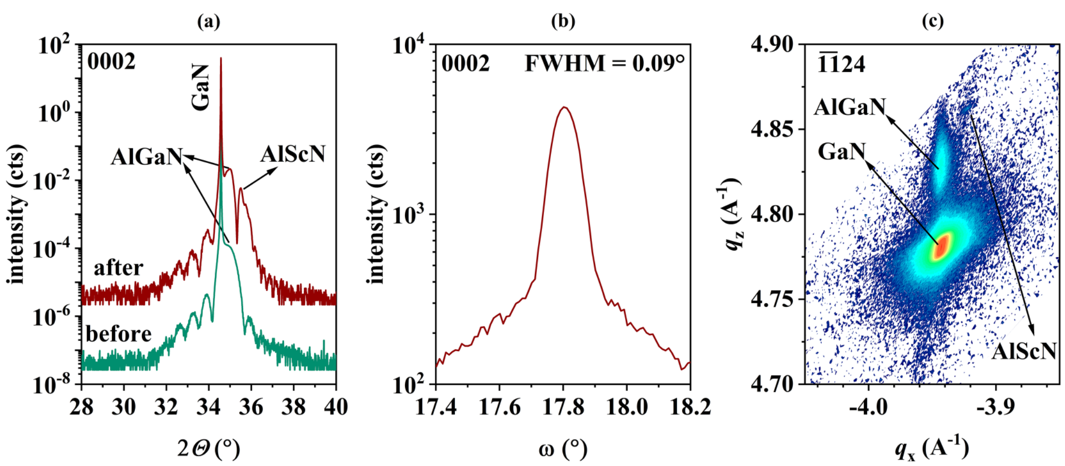

FIG. 2. (a) Symmetric θ/2θ-scans HRXRD of the 0002 reflection of the grown AlGaN/GaN heterostructures before (green curve) and after (red curve) sputtering of the $Al_{0.7}Sc_{0.3}N$ layer. (b) 0002 rocking curve of the $Al_{0.7}Sc_{0.3}N$ layer. The FWHM is indicated at the top right corner. (c) RSM of the $\overline{11}24$ reflection range of the $Al_{0.7}Sc_{0.3}N/Al_{0.3}Ga_{0.7}N$/GaN heterostructure.

compositional uniformity is a significant advantage of the sputtering process, especially when compared to MOCVD. AlScN barrier layers grown with MOCVD often suffer from pronounced compositional grading, a consequence of the low vapor pressure of scandium precursors and elevated growth temperatures required for the process.[17,20] These limitations are less relevant in sputter-deposited AlScN, highlighting the potential of this method for achieving high-quality, compositionally uniform dielectric layers within III-nitride heterostructures.

Moreover, the profile indicates a more gradual transition from AlScN to AlGaN, particularly in the scandium signal, which exhibits a noticeable tail into the AlGaN layer. This behavior is indicative of Sc diffusion into the AlGaN layer, likely induced by high-energy particle bombardment during the sputtering process. However, the Sc signal remains low at the AlGaN/GaN interface, indicating minimal penetration into the GaN layer; this is consistent with XRD findings and confirms the preserved interface quality essential for optimal 2DEG properties in III-nitride heterostructures.

To support these findings and gain further insights into the interface quality, capacitance–voltage (C–V) measurements were performed, focusing on depletion and dielectric behavior. The measurements were conducted using a mercury probe with a diameter of 760 μm via an Agilent Model E4980A LCR meter, with an applied AC signal of 10 kHz frequency and 50 mV amplitude. Figure 4 reveals the C–V profiles obtained from the heterostructures both with and without the AlScN dielectric layer.

In C–V profiles, an abrupt interface is characterized by a sharply defined transition from accumulation to depletion over a narrow voltage range. Both HEMT structures, with and without AlScN, demonstrated such sharp transitions without observable pinch-off issues, indicative of uniform channel depletion and the absence of parasitic channels. This behavior was further supported by G/ω measurements, where both structures exhibited a pronounced G/ω peak at the transition from accumulation to depletion, highlighting the quality and abruptness of the interface. The reduction in capacitance and the rise in the threshold voltage (absolute value) observed after sputtering are attributable to the increased thickness of the composite barrier.

Additionally, the interface trap density was qualitatively assessed through the analysis of hysteresis in the C–V characteristics measured under forward and reverse voltage sweeps. The reference structure exhibited minimal hysteresis, corresponding to a relatively low interface trap density. Notably, the heterostructure incorporating sputtered AlScN showed a reduction in hysteresis, also indicative of preserved interface quality, and suggests that the AlScN layer provides an effective passivation effect.

The influence of the sputtered AlScN layer on the electric properties both HEMT structures was further analyzed using eddy-current sheet resistance measurements and contactless Hall measurements with a Semilab contactless mobility mapper. The measurements were performed at 17 equidistant points across the 4 in. wafer. Figure 5 presents the in-plane mapping of the sheet carrier density (n_s), electron mobility (μ), and sheet resistance (R_{sh}) for the heterostructure incorporating a 25 nm sputtered AlScN layer. The resultant mean values of R_{sh}, n_s, and μ, for both the reference and AlScN/AlGaN/GaN heterostructure, including standard deviations are summarized in Table I.

The reference AlGaN/GaN heterostructure exhibits a sheet resistance of approximately 400 Ω/sq, with an n_s of 1.5×10^{13} cm^{-2} and a μ of 1050 cm^2/V s. In contrast, the introduction of an AlScN dielectric layer leads to a 23% increase in the sheet carrier density, while the mobility decreases to 765 cm^2/V s. Interestingly, AlScN incorporation increased the standard deviation of sheet carrier density and mobility, indicating a greater in-plane variation across the wafer. These variations are speculated to stem from local strain non-uniformities due to structural defects at the AlScN/AlGaN interface, as XRR confirmed uniform AlScN thickness. Further investigations are required to confirm this hypothesis. Nevertheless, the observed mean values in Table I are consistent with recent reports, which similarly revealed an enhanced sheet carrier density and reduced mobility after the deposition of the AlScN layer on AlGaN/GaN heterostructures.[30,31,37] The observed reduction in

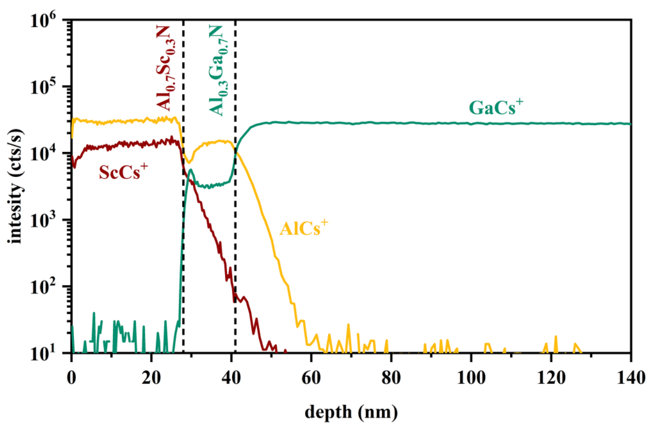

FIG. 3. ToF-SIMS depth profile of a 25 nm sputtered $Al_{0.7}Sc_{0.3}N$ on a GaN-based heterostructure with a 13 nm $Al_{0.3}Ga_{0.7}N$ barrier layer.

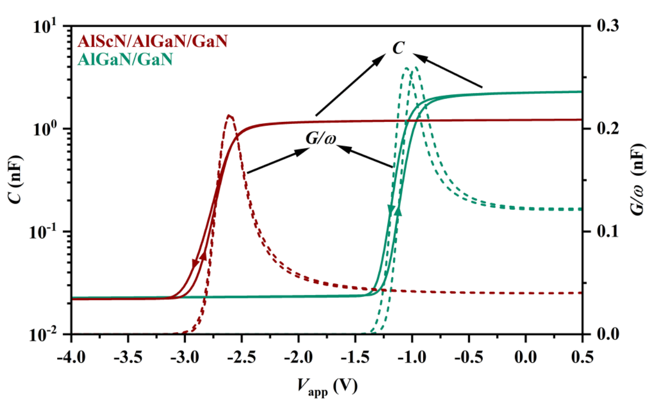

FIG. 4. Capacitance–voltage (C–V) profiles of the $Al_{0.3}Ga_{0.7}N$/GaN HEMT structure before (green line) and after (red) the deposition of an $Al_{0.7}Sc_{0.3}N$ layer on top. The dashed curves represent the corresponding G/ω profiles.

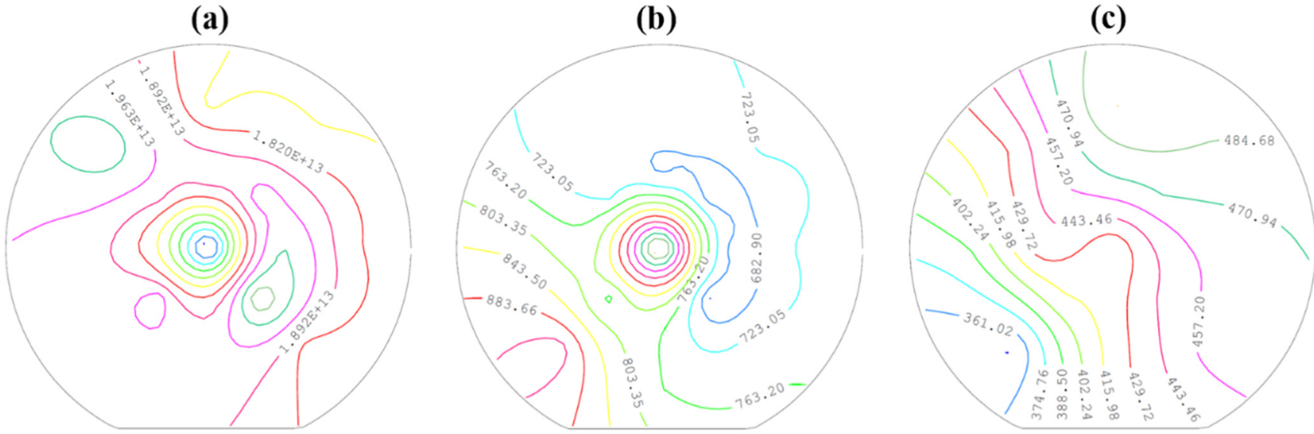

FIG. 5. Electrical property mapping across a 4 in. $Al_{0.3}Ga_{0.7}N$/GaN heterostructure wafer with a 25 nm sputtered $Al_{0.7}Sc_{0.3}N$ layer showing (a) sheet carrier density in cm^{-2}, (b) electron mobility in cm^2/V s, and (c) sheet resistance in Ω/sq. The corresponding average values are listed in Table I.

mobility in the present heterostructures may be attributed to Sc diffusion into the barrier layer, as illustrated in Fig. 3.

Moreover, Okuda *et al.*[30] reported that for Sc concentrations exceeding 6%, the electrical properties of the 2DEG deteriorate significantly, attributing this degradation to defect formation within the AlScN layer or at the regrown interfaces. However, in the current study, such pronounced degradation was not observed. Heterostructures incorporating sputtered $Al_{0.7}Sc_{0.3}N$ maintained a relatively low sheet resistance, exhibiting only a modest increase in the order of 10%, despite the altered mobility.

For comparison, the sheet carrier density of AlScN/AlGaN/GaN and AlGaN/GaN heterostructures was determined as a function of AlScN and AlGaN barrier thickness, respectively, using the 1D Schrödinger–Poisson solver nextnano (see Fig. 6). In defect-free structures, the sheet carrier density is expected to increase with barrier thickness,[9] a trend clearly observed in the simulations (solid lines). Interestingly, the AlScN/AlGaN/GaN structures exhibit a distinct behavior with a sudden onset of increased sheet carrier density when the AlScN thickness is around 3–4 nm due to the formation of a second 2DEG channel at the AlScN/AlGaN interface. In this case, the sum of the 2DEG densities at these interfaces was used as the sheet carrier density for the defect-free AlScN/AlGaN/GaN heterostructures (red solid line).

Compared to a 30 nm AlGaN/GaN reference, the AlScN/AlGaN/GaN structure with equivalent total barrier thickness (AlScN (17 nm)/AlGaN (13 nm)) exhibits a simulated sheet carrier density that is around 2.5 times higher, demonstrating the significant potential of composite barriers. However, the experimental values (Table I) reveal that while the AlGaN/GaN sheet carrier density aligns well with simulations, the AlScN/AlGaN/GaN density is substantially lower than predicted.

A possible reason for this observation could be an alteration of the polarization quantities. The simulated values were calculated based on the assumption that the AlScN layer is coherently strained to the GaN layer, which does not occur in the characterized heterostructures due to the observed relaxation in the AlScN layer [see Fig. 2(c)]. Indeed, reducing the polarization gradient formed at the AlScN/AlGaN interface from 0.0664 to 0.0042 C/m^2 causes the simulated sheet carrier density (red dashed line) to match the experimental value. While the difference is mainly attributed to the alteration in the polarization gradient at the AlScN/AlGaN interface due to AlScN relaxation, the influence of sputtering-induced interfacial defects cannot be entirely ruled out. Nevertheless, despite this observation, the sheet carrier density still shows an improvement, even though not as significant as theoretically predicted for coherent growth, when compared to the AlGaN/GaN structures without AlScN layers. These results highlight the potential of sputtered AlScN layers, even with Sc concentrations up to 30%, as a dielectric to enhance the performance and tunability of AlGaN/GaN heterostructures.

III. DEVICE FABRICATION AND PERFORMANCE CHARACTERIZATION AlGaN/GaN HEMT WITH A SPUTTERED AlScN GATE DIELECTRIC

HEMTs with AlScN barriers present considerable opportunities for outperforming the current GaN-based HEMTs.[1] Recent studies on MBE- and MOCVD-grown AlScN barriers demonstrate

TABLE I. The average R_{sh}, μ, and n_s obtained across the 4 in. wafers by contactless Hall measurements.

Sample	R_{sh} (Ω/sq)	μ (cm^2/V s)	n_s (10^{13} cm^{-2})
GaN/$Al_{0.3}Ga_{0.7}N$/GaN	406 ± 4	1043 ± 17	1.47 ± 0.03
$Al_{0.7}Sc_{0.3}N$/$Al_{0.3}Ga_{0.7}N$/GaN	441 ± 37	765 ± 119	1.89 ± 0.18

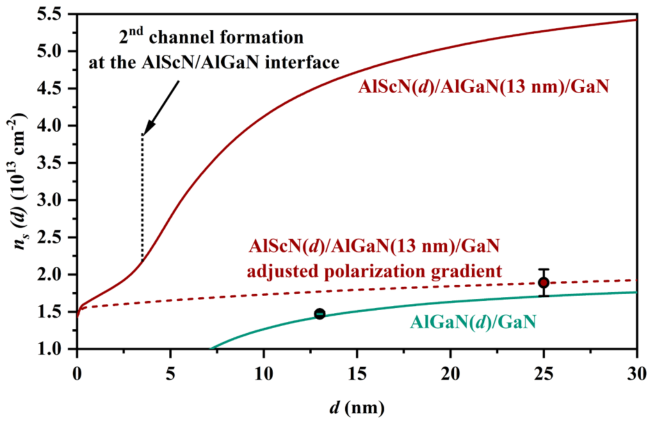

FIG. 6. Comparison of the measured sheet carrier density (n_s) [red circle: AlScN/AlGaN/GaN heterostructure; green circle: AlGaN/GaN reference (see Table I)] with simulated sheet carrier densities as a function of barrier thickness for defect-free $Al_{0.3}Ga_{0.7}N/GaN$ (green solid line) and $Al_{0.7}Sc_{0.3}N/Al_{0.3}Ga_{0.7}N$ (13 nm)/GaN (red solid line) heterostructures, calculated using the 1D Schrödinger–Poisson solver nextnano. The material parameters used for the simulation follow those reported in Refs. 7, 9, 10, and 38–41. The vertical black dotted line indicates the AlScN thickness (3–4 nm) at which a second 2DEG channel forms at the AlScN/AlGaN interface. The red solid line represents the total sheet carrier density (sum of both 2DEG channels). The red dashed line shows the simulation of the AlScN/AlGaN (13 nm)/GaN adjusted for reduced polarization gradient at the AlScN/AlGaN interface.

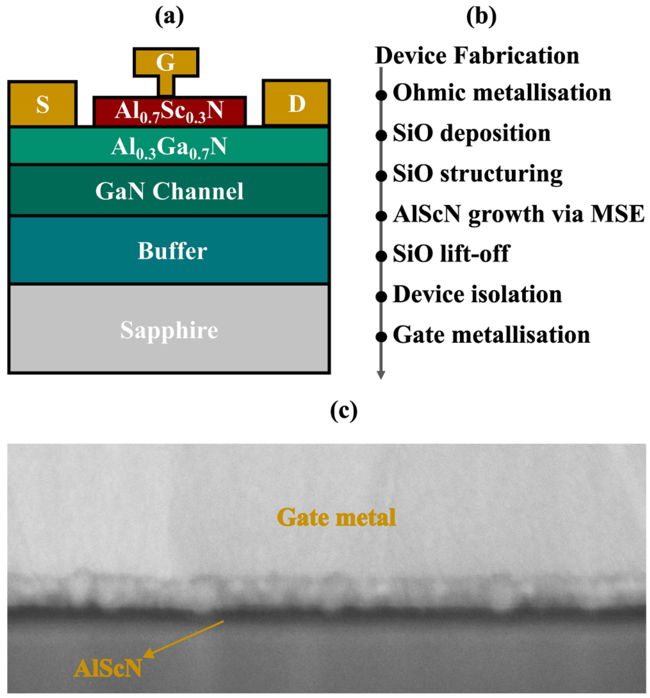

FIG. 7. (a) Schematic representation of the $Al_{0.3}Ga_{0.7}N/GaN$ HEMT device structure incorporating an $Al_{0.7}Sc_{0.3}N$ gate dielectric layer deposited by magnetron sputter epitaxy (MSE). (b) Overview of the key device fabrication steps. (c) Cross-sectional SEM image of the gate region in the fabricated AlScN/AlGaN/GaN HEMT.

promising advancements, particularly in achieving elevated transistor current densities.[13,14,19] Additionally, Yin *et al.*[37] observed an increased two-dimensional electron gas (2DEG) density in devices employing an MBE-grown AlScN/AlGaN composite barrier. Similar findings were reported by Okuda *et al.*[30] and Ota *et al.*,[31] and reflected in the present results, even when sputtered AlScN layers are employed. However, the demonstration of this enhancement at the transistor level for composite barriers is still lacking.

To investigate whether the observed increase in the sheet carrier density in heterostructures with a composite barrier translates into enhanced saturation currents, transistors were fabricated. Achieving low resistance ohmic contacts is essential to fully exploit the device potential; however, this remains a significant challenge for AlScN barriers.[1] This is a general issue for HEMTs possessing a barrier material with elevated Al concentration.[42,43] An increase in the Al mole fraction reduces the electron affinity of the barrier, thereby raising the Schottky barrier height at the metal–semiconductor interface.[1,43] This increased barrier height limits electron tunneling and thermionic emission. Additionally, at very high Al concentrations, the barrier material strongly suppresses the ionization of common n-type dopants, owing to deeper donor levels and lower carrier activation efficiencies.[1] These effects limit the realization of low-resistance ohmic contacts in HEMTs with a high Al-content barrier. The heterostructures investigated in this work comprise a composite barrier stack of AlScN and AlGaN, specifically entailing an AlScN layer with a relatively high Al concentration of approximately 70%, combined with an AlGaN layer possessing a lower Al concentration close to 30%. Given these compositional considerations, it is advantageous to preferentially form ohmic contacts on the AlGaN layer rather than directly on the AlScN.

A practical and straightforward approach to achieving this selective contact formation involves the precise removal of the AlScN layer via etching to expose the underlying AlGaN layer. However, this approach is complicated by the etching characteristics of AlScN. Dry etching methods, particularly for AlScN layers with high Sc fractions, generally exhibit low etch rates and poor process control.[44] Conversely, wet etching offers several effective chemical based solutions (NH_4OH, KOH, or TMAH) for the removal of AlScN, but it remains susceptible to challenges such as anisotropy related to material polarity, difficulty in controlling undercut beneath the resist mask, and maintaining an optimal surface roughness post-etch.[45] These factors critically influence the quality and reproducibility of the subsequent metallization and contact performance.[46]

To tackle this challenge, the formation of the ohmic contact was implemented prior to the local deposition of the AlScN layer. The main device fabrication steps are illustrated in Fig. 7(a). The process starts with the structuring and e-beam evaporation of Ti/Al-based ohmic contacts. This was followed by an annealing step aimed at improving the electrical characteristics of the contacts.

Subsequently, a silicon oxide (SiO) sacrificial layer was deposited, and openings corresponding to the AlScN layer in the gate region were defined via stepper lithography. The AlScN layer was then deposited by magnetron sputter epitaxy (MSE) under the growth conditions specified in Sec. II. Afterward, the SiO mask was removed using a lift-off process. Device isolation was achieved through Ar-ion implantation. The fabrication was resumed by depositing Ni/Pt/Au as gate metal contacts. Although not shown in Fig. 7, the fabrication process is completed by an SiN passivation layer deposited by plasma enhanced chemical vapor deposition (PECVD), via etching and metal interconnects. Figure 7(c) reveals an SEM image of a cross section of the gate region of the processed AlScN/AlGaN/GaN HEMT. A distinct AlScN layer beneath the gate metal is clearly present as shown in the enlarged gate image. For the reference AlGaN/GaN HEMT, the same steps were performed. The only exception was the step involving AlScN sputtering.

To investigate the impact of the AlScN layer on transistor performance, static and pulsed DC measurements were conducted and compared with those of the reference HEMT structure. The measured transistors featured a gate length and a gate width of 1 and 50 μm, respectively, with gate-to-source of 1 μm and gate-to-drain spacings of 1.5 μm. Figure 8 reveals the static DC transfer characteristics of both devices. The reference device exhibits a current density ($I_{DS,sat}$) of approximately 0.70 A/mm at a gate-to-source voltage (V_{GS}) of 2 V. At the same bias, the HEMT featuring the composite AlScN/AlGaN barrier achieves a saturation current density of around 0.88 A/mm, representing an increase of nearly 25% compared to the reference structure. A comparable increase was observed in the sheet carrier density (n_s), indicating that the observed enhancement in $I_{DS,sat}$ is predominantly attributable to the elevated carrier density. Although the achieved current levels remain below those reported for sub-100 nm HEMTs with purely AlScN barriers,[13,14,19] these findings clearly demonstrate the potential offered by composite barriers.

The transfer characteristic of the composite barrier device further shows a smooth and well-defined transition from the on-state to the off-state [see Fig. 8(a)], consistent with the C–V measurements, thereby indicating the absence of pinch-off instabilities and parasitic channel formation, which contrasts with the behavior reported for HEMTs employing MOCVD-grown AlScN barriers.[22] Additionally, it is worth noting that the composite barrier device achieves an I_{on}/I_{off} ratio of approximately 10^7, which is higher than those reported for devices employing only AlScN barriers,[14] thereby indicating the superior electrical insulating properties of AlScN layers deposited by magnetron sputter epitaxy. Furthermore, these devices display even lower leakage currents compared to the reference HEMT. These results highlight the potential of MSE-grown AlScN to function effectively as both a passivation layer and a barrier material, underscoring the important role this technique could play in the advancement of high-performance HEMTs.

Moreover, a pronounced decrease in the transconductance (g_m) is observed, dropping from 0.32 S/mm in the reference device to 0.16 S/mm in the HEMT with the composite barrier. Transconductance is known to be influenced by various factors including carrier mobility, barrier thickness, parasitic resistances, and interface quality.[11,47] While the contributions of these factors cannot be entirely excluded, the increased barrier thickness of the composite structure (approximately 40 nm) appears to be the probable cause of this reduction. This also likely explains the strong negative shift in threshold voltage (V_{th}) from −0.8 to −7.8 V observed in the composite barrier device.

Figures 9(a) and 9(b) present the pulsed DC output characteristics (0.5 ms pulse width, 0.5% duty cycle) for the reference HEMT and the composite barrier HEMT, respectively. To account for the distinct threshold voltages of each device, different V_{GS} bias ranges were applied, spanning from the off-state to the saturation drain current. The reference HEMT was swept from −2 to 2 V in 0.4 V steps, while the composite barrier HEMT was swept from −8 to 2 V in 1 V steps. Consistent with the transfer characteristics, the composite barrier HEMT attains a higher $I_{DS,sat}$ than the reference device. Additionally, a marked degradation in the I_{DS} curve is observed for the reference HEMT at high V_{GS}, which can be attributed to increased forward gate current due to gate turn-on (see Fig. 8). Despite the higher sheet carrier density in the composite barrier HEMT, its on-resistance (R_{ON}) is elevated by approximately 25%.

Typically, R_{ON} is closely correlated with sheet resistance (R_{sh}),[42] and indeed, a 10% increase in R_{sh} was observed in heterostructures incorporating the sputtered AlScN dielectric (Table I). However, this modest rise is not sufficient to explain the substantial increase in R_{ON}. Another key parameter potentially affecting R_{ON} is the contact resistance.[48] Although the ohmic contacts were fabricated before the deposition of AlScN, which would typically suggest similar contact resistance in both devices, the median contact resistance measured for the AlScN-based HEMT was 0.18 Ω mm, higher than that of the reference device, which showed a contact resistance of 0.11 Ω mm. These observations suggest that the increase in R_{ON} can be associated with the elevated contact resistance observed in the composite barrier device. Although the AlGaN/GaN heterostructures were passivated with a SiO mask, the sputtering process still negatively affected the contacts. Nevertheless, this approach remains promising, as the achieved contact resistance is significantly lower compared to directly placing ohmic contacts on the AlScN layer.[19] Further improvement can be expected by fine-tuning the MSE growth parameters, for instance, by optimizing the AlScN layer thickness.

In order to investigate this approach and study the influence of AlScN gate dielectric thickness on key device parameters, two additional devices were fabricated following the process outlined in Fig. 7. Based on the growth rate, the growth time was adjusted to produce devices with AlScN layer thicknesses of 15 and 20 nm. Figure 10 presents key device parameters including saturation current, maximum transconductance, threshold voltage, and on-resistance as a function of AlScN layer thickness. For this analysis, devices with a gate length of 0.7 μm, a gate width of 50 μm, a gate-to-source of 1 μm, and gate-to-drain spacings of 3 μm were considered.

As observed, $I_{DS,sat}$ exhibits a clear increasing trend with increasing AlScN layer thickness, reaching its highest value for transistors incorporating a 25 nm AlScN layer. The saturation current increased from 0.82 A/mm in the reference HEMT to nearly 0.90 A/mm for devices with a 15 nm layer and further to 0.98 A/mm for those with a 25 nm AlScN barrier. This enhancement is likely attributable to the expected increase in the sheet

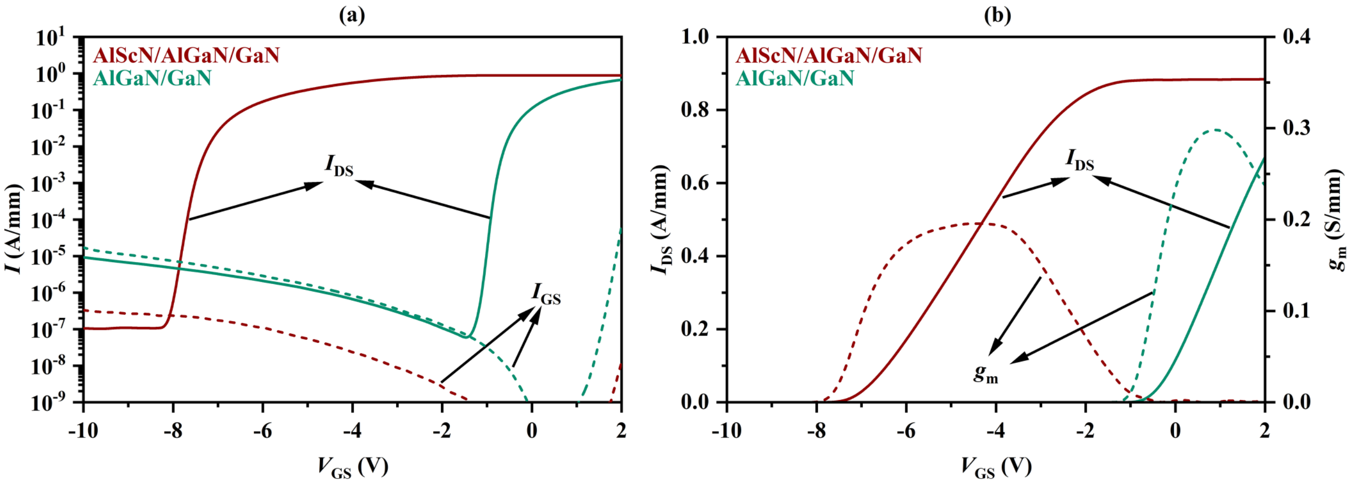

FIG. 8. (a) Semi-logarithmic I–V characteristics and (b) DC transfer curves measured at $V_{DS} = 2.5$ V for AlGaN/GaN HEMT devices with (red) and without (green) a sputtered AlScN gate dielectric. The transistors feature a gate length of 1 μm and a gate width of 50 μm, with gate-to-source and gate-to-drain spacings of 1 and 1.5 μm, respectively.

carrier density due to reduced depletion effects at the Schottky contact as the barrier thickness increases.[9]

In contrast, as anticipated, $g_{m,max}$ exhibits an inverse relationship with AlScN thickness, decreasing as the layer becomes thicker. Importantly, the reduction in $g_{m,max}$ after deposition of the 15 nm AlScN layer remains modest compared to the reference device, indicating minimal compromise in transconductance performance at this thickness.

Similar to the observed trend in $I_{DS,sat}$, the absolute value of V_{th} increases with increasing AlScN layer thickness. Interestingly, V_{th} shows only a slight increase for dielectric thicknesses from 0 up to 20 nm, followed by a pronounced rise at 25 nm. While a general increase in V_{th} with layer thickness is expected,[49] the significant jump at 25 nm is noteworthy. The underlying cause of this behavior remains unclear; however, it is speculated that AlScN layers thinner than 25 nm are not completely closed, potentially

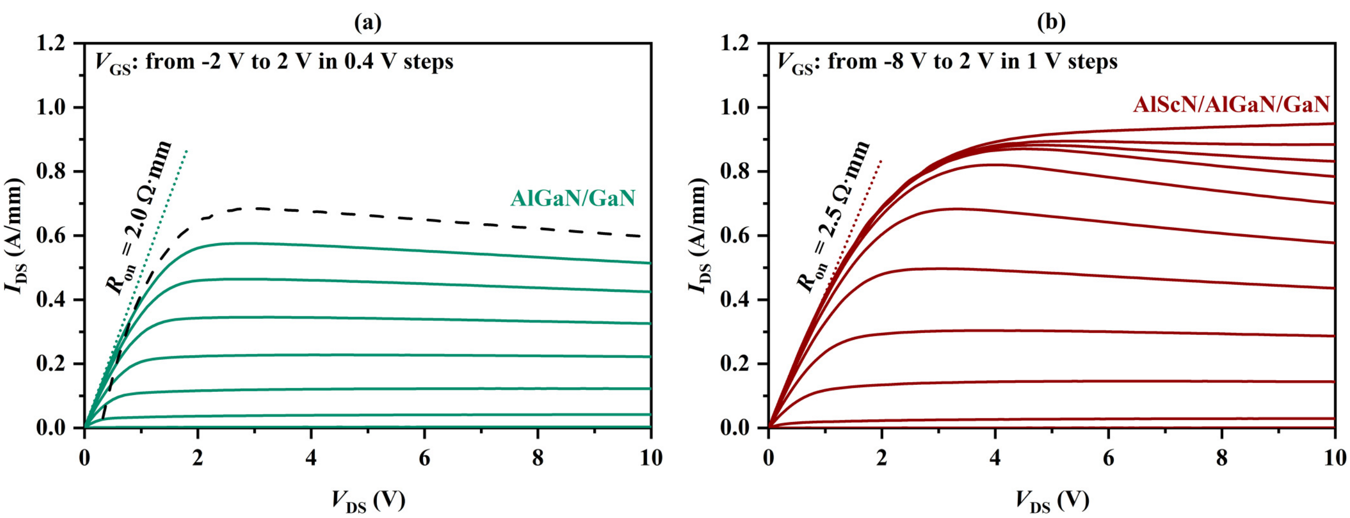

FIG. 9. Pulsed DC output characteristics of AlGaN/GaN HEMT devices are shown for (a) device without and (b) device with a sputtered AlScN gate dielectric. Each transistor features a gate length of 1 μm, gate width of 50 μm, gate-to-source distance of 1 μm, and gate-to-drain distance of 1.5 μm. Due to the pronounced difference in V_{th}, AlGaN/GaN HEMT was characterized with V_{GS} ranging from −2 to 2 V in 0.4 V steps, whereas AlScN/AlGaN/GaN HEMT was measured from −8 to 2 V in 1 V steps. The dashed black line in (a) highlights a deterioration in the I_{DS} characteristic at $V_{GS} = 2$ V, related to increased gate current (see Fig. 8).

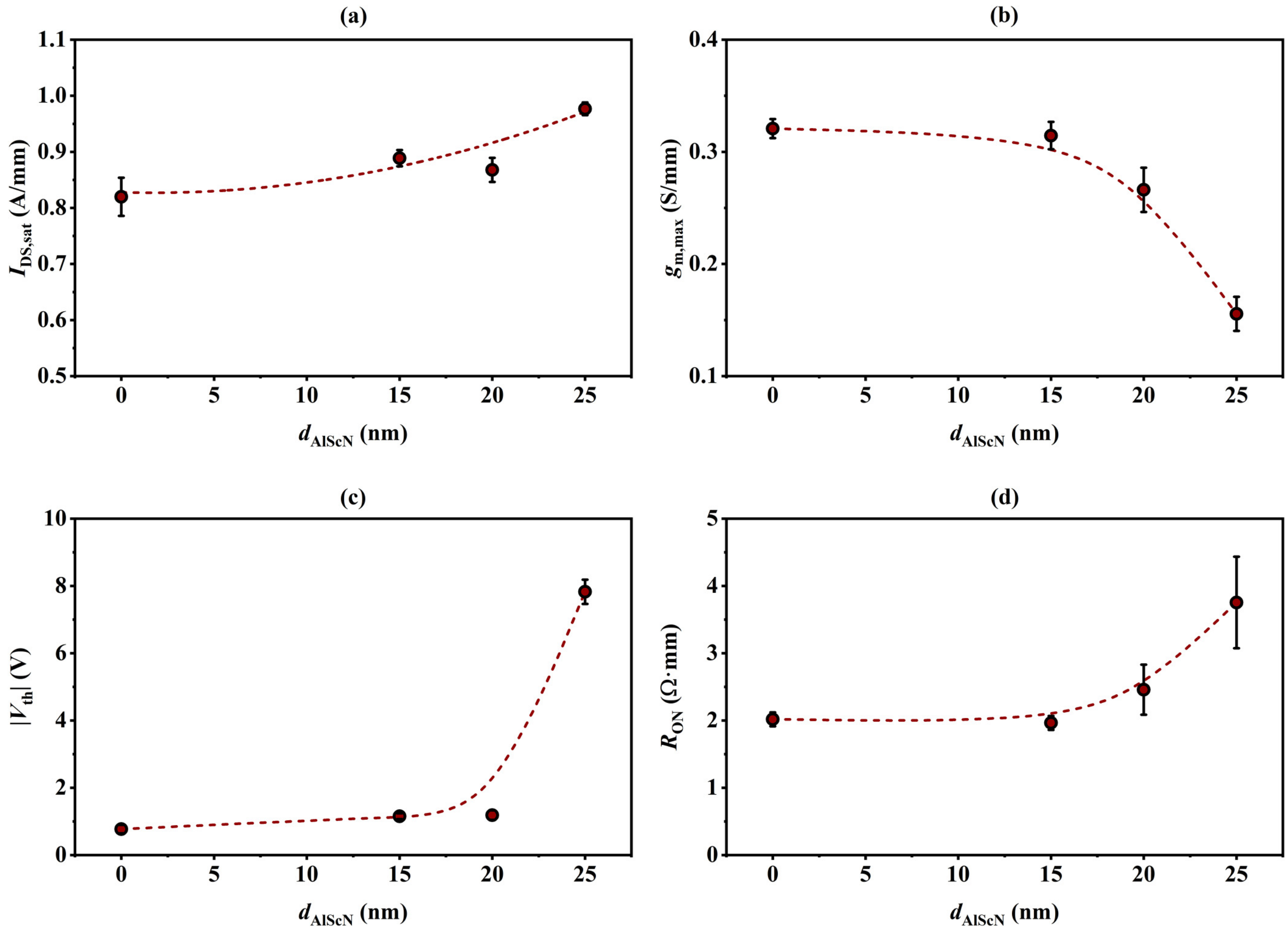

FIG. 10. Key device parameters as a function of AlScN layer thickness d_{AlScN} including (a) saturation current $I_{DS,sat}$, (b) maximum transconductance $g_{m,max}$, (c) threshold voltage V_{th}, and (d) on-resistance R_{on}. The transistors feature a gate length of 0.7 μm, gate width of 50 μm, and gate-to-source and gate-to-drain spacings of 1 and 3 μm, respectively.

containing voids (which are absent in layers with 25 nm thickness, as shown in Fig. 1). These voids likely alter the surface potential or even the potential at the AlScN/AlGaN interface, thereby influencing V_{th}. Although direct correlation studies are currently lacking, it is well known that surface morphology and surface states strongly impact threshold voltage.[50] Further investigations are needed to verify this hypothesis and clarify the origin of the significant V_{th} increase.

Moreover, R_{ON} also demonstrates an increasing trend with greater AlScN thickness, rising from 2 Ω mm in the reference device to 3.5 Ω mm for the device with a 25 nm AlScN gate dielectric. Notably, R_{ON} at 15 nm remains nearly unchanged compared to the reference. These results support the assumption that reducing the sputtered AlScN layer thickness is beneficial for maintaining low R_{ON}.

To further assess the impact of the sputtered AlScN layer on HEMT performance, the off-state leakage characteristics were investigated at $V_{GS} = -10$ V with the V_{DS} increasing from 0 V up to the soft-breakdown threshold defined at 1 mA/mm.

The results, illustrated in Fig. 11, reveal that the leakage current initially increases with AlScN thickness, reaching a maximum for devices with a 20 nm AlScN layer, before decreasing upon further increasing the thickness to 25 nm, relative to the reference device. Although multiple factors may contribute to this behavior, it is likely that the observed trend is closely correlated with the notable threshold voltage variation [see Fig. 10(c)] and potentially explained by the incomplete closure of AlScN layers thinner than 25 nm. Despite this observation, the presence of the AlScN layer elevates the voltage at which soft-breakdown occurs even for devices with the 20 nm AlScN layer (highest leakage), indicating enhanced device robustness. These findings further underscore the effectiveness of the AlScN layer as a passivation layer, contributing to improved off-state reliability and breakdown

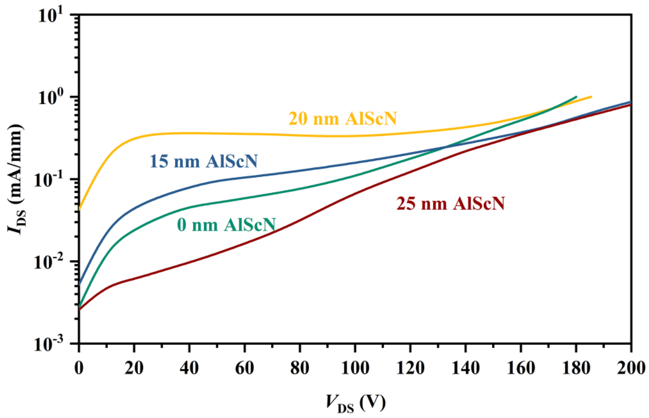

FIG. 11. Off-state leakage characteristics of devices with sputtered AlScN gate dielectrics of varying thicknesses, measured up to the soft-breakdown limit of 1 mA/mm at V_{GS} = −10 V. The device with the 0 nm AlScN layer represents the reference AlGaN/GaN. All transistors have gate length of 1 μm, gate width of 50 μm, gate-to-source distance of 1 μm, and gate-to-drain distance of 1.5 μm.

behavior in the HEMTs. Overall, the evaluation of the key device parameters shown in Figs. 10 and 11 indicates that transistors with a 15 nm AlScN layer achieve the most favorable balance, exhibiting the most attractive DC performance among all devices studied.

IV. CONCLUSION

In this study, the effect of sputtered $Al_{0.7}Sc_{0.3}N$ layers on AlGaN/GaN heterostructures and HEMT performance was systematically investigated. At the heterostructure level, AlScN deposition preserved surface smoothness and interface quality, as confirmed by HRXRD and AFM, despite the observed relaxation of the AlScN layer attributed to suboptimal growth conditions. Uniform composition was achieved, even though limited Sc diffusion into AlGaN occurred. However, the barrier/GaN interface remained preserved, ensuring reliable electronic properties, as supported by C–V measurements showing uniform channel depletion. The AlScN layer also reduced C–V hysteresis, indicating an effective passivation effect. The sheet carrier density n_s increased from 1.4 to 1.89×10^{13} cm^{-2}, though accompanied by reduced mobility. At the device level, HEMTs with a 0.7 μm gate length exhibited an increase in saturation current from 0.82 to 0.98 A/mm after the deposition of a 25 nm AlScN layer. The composite barrier configuration also results in reduced leakage and improved insulation, but is accompanied by lower transconductance, a pronounced negative shift in threshold voltage, and elevated on-resistance. The increase in R_{on} is likely attributable to greater contact resistance stemming from sputter-induced contact damage. An optimized device with a 15 nm AlScN layer offered the best balance, enhancing saturation current and soft-breakdown voltage while limiting degradation in transconductance and on-resistance. Based on these results, sputtered AlScN proves effective as both a barrier layer and a passivation layer, improving performance and robustness of GaN-based devices when carefully optimized.

ACKNOWLEDGMENTS

This work was partially supported by the German Science Foundation (DFG) project (No. 495652244). In addition, the work was partially supported by the Gips-Schüle-Stiftung and the Federal Ministry of Education and Research (BMBF) via the project "ForMikro-SALSA" (Project-ID: 16ES1053).

AUTHOR DECLARATIONS

Conflict of Interest

The authors have no conflicts to disclose.

Author Contributions

A. Yassine: Conceptualization (lead); Data curation (lead); Formal analysis (lead); Investigation (lead); Methodology (lead); Validation (lead); Visualization (lead); Writing – original draft (lead); Writing – review & editing (lead). **R. Driad:** Data curation (equal); Formal analysis (supporting); Investigation (supporting); Methodology (equal); Validation (equal); Visualization (supporting); Writing – review & editing (equal). **A. Nair:** Data curation (supporting); Investigation (supporting); Methodology (supporting); Validation (supporting); Visualization (supporting). **P. Ott:** Data curation (supporting); Investigation (supporting); Methodology (supporting); Validation (supporting); Visualization (supporting); Writing – review & editing (supporting). **L. Kirste:** Data curation (supporting); Methodology (supporting). **P. Straňák:** Data curation (supporting); Methodology (supporting). **H. Czap:** Data curation (supporting); Methodology (supporting). **M. Mikulla:** Funding acquisition (equal); Project administration (equal); Resources (equal). **M. Yassine:** Formal analysis (equal); Supervision (supporting); Validation (supporting); Visualization (supporting); Writing – review & editing (equal). **O. Ambacher:** Conceptualization (supporting); Formal analysis (supporting); Funding acquisition (lead); Investigation (supporting); Project administration (lead); Resources (equal); Supervision (lead); Validation (equal); Visualization (supporting); Writing – review & editing (equal).

DATA AVAILABILITY

The data that support the findings of this study are available from the corresponding author upon reasonable request.

REFERENCES

[1] M. T. Hasan and Z. Mi, APL Electron. Devices **1**, 021507 (2025).
[2] M. Hardy, D. Meyer, N. Nepal, B. Downey, D. S. Katzer, and D. Storm, in *2018 IEEE MTT-S International Microwave Workshop Series on Advanced Materials and Processes for RF and THz Applications (IMWS-AMP)* (IEEE, 2018)), pp. 1–3.
[3] S. Zhang, W. Y. Fu, D. Holec, C. J. Humphreys, and M. A. Moram, J. Appl. Phys. **114**, 243516 (2013).
[4] D. V. Dinh, J. Lähnemann, L. Geelhaar, and O. Brandt, Appl. Phys. Lett. **122**, 152103 (2023).
[5] L. van Deurzen, T.-S. Nguyen, J. Casamento, H. G. Xing, and D. Jena, Appl. Phys. Lett. **123**, 241104 (2023).
[6] K. Furuta, K. Hirata, S. A. Anggraini, M. Akiyama, M. Uehara, and H. Yamada, J. Appl. Phys. **130**, 024104 (2021).

[7]H. Wang, N. Adamski, S. Mu, and C. G. Van de Walle, J. Appl. Phys. **130**, 104101 (2021).
[8]M. Akiyama, T. Kamohara, K. Kano, A. Teshigahara, Y. Takeuchi, and N. Kawahara, Adv. Mater. **21**, 593 (2009).
[9]O. Ambacher, B. Christian, M. Yassine, M. Baeumler, S. Leone, and R. Quay, J. Appl. Phys. **129**, 204501 (2021).
[10]O. Ambacher, A. Yassine, M. Yassine, S. Mihalic, E. Wade, and B. Christian, J. Appl. Phys. **131**, 245702 (2022).
[11]P. Döring, S. Krause, C. Friesicke, and R. Quay, IEEE Trans. Electron Devices **71**, 1670 (2024).
[12]M. T. Hardy, B. P. Downey, N. Nepal, D. F. Storm, D. S. Katzer, and D. J. Meyer, Appl. Phys. Lett. **110**, 162104 (2017).
[13]T. E. Kazior, E. M. Chumbes, B. Schultz, J. Logan, D. J. Meyer, and M. T. Hardy, in *2019 IEEE MTT-S International Microwave Symposium (IMS)* (IEEE, 2019), pp. 1136–1139.
[14]K. Nomoto, J. Casamento, T. S. Nguyen, L. Li, H. Lee, C. Savant, A. L. Hickman, T. Maeda, J. Encomendero, V. Gund, T. Vasen, S. Afroz, D. Hannan, J. C. M. Hwang, D. Jena, and H. G. Xing, Appl. Phys. Express **18**, 016506 (2025).
[15]J. Ligl, S. Leone, C. Manz, L. Kirste, P. Doering, T. Fuchs, M. Prescher, and O. Ambacher, J. Appl. Phys. **127**, 195704 (2020).
[16]I. Streicher, S. Leone, L. Kirste, C. Manz, P. Straňák, M. Prescher, P. Waltereit, M. Mikulla, R. Quay, and O. Ambacher, Phys. Status Solidi RRL **17**, 2200387 (2022).
[17]I. Streicher, S. Leone, M. Zhang, T. S. Tlemcani, M. Bah, P. Straňák, L. Kirste, M. Prescher, A. Yassine, D. Alquier, and O. Ambacher, Adv. Funct. Mater. **34**, 2403027 (2024).
[18]C. Manz, S. Leone, L. Kirste, J. Ligl, K. Frei, T. Fuchs, M. Prescher, P. Waltereit, M. A. Verheijen, A. Graff, M. Simon-Najasek, F. Altmann, M. Fiederle, and O. Ambacher, Semicond. Sci. Technol. **36**, 034003 (2021).
[19]S. Krause, I. Streicher, P. Waltereit, L. Kirste, P. Bruckner, and S. Leone, IEEE Electron Device Lett. **44**, 17 (2023).
[20]I. Streicher, S. Leone, C. Manz, L. Kirste, M. Prescher, P. Waltereit, M. Mikulla, R. Quay, and O. Ambacher, Cryst. Growth Des. **23**, 782 (2023).
[21]A. Yassine, M. Yassine, I. Streicher, R. Driad, L. Kirste, P. Straňák, P. Döring, S. Leone, and O. Ambacher, J. Appl. Phys. **137**, 194501 (2025).
[22]P. Döring, S. Krause, P. Waltereit, P. Brückner, S. Leone, I. Streicher, M. Mikulla, and R. Quay, Appl. Phys. Lett. **123**, 032101 (2023).
[23]J. Casamento, H. Lee, C. S. Chang, M. F. Besser, T. Maeda, D. A. Muller, H. G. Xing, and D. Jena, APL Mater. **9**, 091106 (2021).
[24]P. Wang, D. Wang, Y. Bi, B. Wang, J. Schwartz, R. Hovden, and Z. Mi, Appl. Phys. Lett. **120**, 012104 (2022).
[25]J. Casamento, T. S. Nguyen, Y. Cho, C. Savant, T. Vasen, S. Afroz, D. Hannan, H. G. Xing, and D. Jena, Appl. Phys. Lett. **121**, 192101 (2022).
[26]N. Izyumskaya, V. Avrutin, K. Ding, Ü. Özgür, H. Morkoç, and H. Fujioka, Semicond. Sci. Technol. **34**, 093003 (2019).
[27]J. Casamento, S. M. Baksa, D. Behrendt, S. Calderon, D. Goodling, J. Hayden, F. He, L. Jacques, S. H. Lee, W. Smith, A. Suceava, Q. Tran, X. Zheng, R. Zu, T. Beechem, I. Dabo, E. C. Dickey, G. Esteves, V. Gopalan, M. D. Henry, J. F. Ihlefeld, T. N. Jackson, S. V. Kalinin, K. P. Kelley, Y. Liu, A. M. Rappe, J. Redwing, S. Trolier-McKinstry, and J.-P. Maria, Appl. Phys. Lett. **124**, 080501 (2024).
[28]A. Kobayashi, Y. Honda, T. Maeda, T. Okuda, K. Ueno, and H. Fujioka, Appl. Phys. Express **17**, 011002 (2024).
[29]G. Schönweger, A. Petraru, M. R. Islam, N. Wolff, B. Haas, A. Hammud, C. Koch, L. Kienle, H. Kohlstedt, and S. Fichtner, Adv. Funct. Mater. **32**, 2109632 (2022).
[30]T. Okuda, S. Ota, T. Kawahara, K. Makiyama, K. Nakata, T. Maeda, and A. Kobayashi, Appl. Phys. Lett. **126**, 052105 (2025).
[31]S. Ota, T. Okuda, K. Kubota, Y. Wakamoto, T. Maeda, T. Kawahara, K. Makiyama, K. Nakata, and A. Kobayashi, APL Mater. **13**, 081112 (2025).
[32]T. Maeda, Y. Wakamoto, K. Kubota, T. Kawahara, S. Yoshida, K. Makiyama, K. Nakata, and A. Kobayashi, in *2025 Device Research Conference (DRC)* (IEEE, 2025), pp. 1–2.
[33]Y. Lu, "Development and characterization of piezoelectric AlScN-based alloys for electroacoustic applications," dissertation (Albert-Ludwigs-Universität Freiburg, Freiburg, 2019).
[34]D. Wang, P. Wang, M. He, J. Liu, S. Mondal, M. Hu, D. Wang, Y. Wu, T. Ma, and Z. Mi, Appl. Phys. Lett. **122**, 090601 (2023).
[35]T.-S. Nguyen, N. Pieczulewski, C. Savant, J. J. P. Cooper, J. Casamento, R. S. Goldman, D. A. Muller, H. G. Xing, and D. Jena, APL Mater. **12**, 101117 (2024).
[36]B. Dzuba, T. Nguyen, A. Sen, R. E. Diaz, M. Dubey, M. Bachhav, J. P. Wharry, M. J. Manfra, and O. Malis, J. Appl. Phys. **132**, 175701 (2022).
[37]Y. Yin, H. Zhao, R. Liu, S. Fan, J. Sun, H. Qin, H. Song, J. Li, S. Dong, Q. Sun, and H. Yang, Appl. Phys. Lett. **125**, 192103 (2024).
[38]S. Zhang, D. Holec, W. Y. Fu, C. J. Humphreys, and M. A. Moram, J. Appl. Phys. **114**, 133510 (2013).
[39]C. E. Dreyer, A. Janotti, C. G. Van de Walle, and D. Vanderbilt, Phys. Rev. X **6**, 021038 (2016).
[40]D. F. Urban, O. Ambacher, and C. Elsässer, Phys. Rev. B **103**, 115204 (2021).
[41]K. R. Talley, S. L. Millican, J. Mangum, S. Siol, C. B. Musgrave, B. Gorman, A. M. Holder, A. Zakutayev, and G. L. Brennecka, Phys. Rev. Mater. **2**, 063802 (2018).
[42]M. Meneghini, C. D. Santi, I. Abid, M. Buffolo, M. Cioni, R. A. Khadar, L. Nela, N. Zagni, A. Chini, F. Medjdoub, G. Meneghesso, G. Verzellesi, E. Zanoni, and E. Matioli, J. Appl. Phys. **130**, 181101 (2021).
[43]A. G. Baca, A. M. Armstrong, B. A. Klein, A. A. Allerman, E. A. Douglas, and R. J. Kaplar, J. Vac. Sci. Technol. A **38**, 020803 (2020).
[44]M. T. Hardy, B. P. Downey, D. J. Meyer, N. Nepal, D. F. Storm, and D. S. Katzer, IEEE Trans. Semicond. Manuf. **30**, 475 (2017).
[45]K. Airola, S. Mertin, J. Likonen, E. Hartikainen, K. Mizohata, J. Dekker, A. Thanniyil Sebastian, and T. Pensala, Materialia **22**, 101403 (2022).
[46]S. Joglekar, M. Azize, M. Beeler, E. Monroy, and T. Palacios, Appl. Phys. Lett. **109**, 041602 (2016).
[47]S. Y. Chou and D. A. Antoniadis, IEEE Trans. Electron Devices **34**, 448 (1987).
[48]W. Saito, T. Suwa, T. Uchihara, T. Naka, and T. Kobayashi, Microelectron. Reliab. **55**, 1682 (2015).
[49]B. K. Ridley, Appl. Phys. Lett. **77**, 990 (2000).
[50]T.-L. Wu, D. Marcon, B. Bakeroot, B. D. Jaeger, H. C. Lin, J. Franco, S. Stoffels, M. Van Hove, R. Roelofs, G. Groeseneken, and S. Decoutere, Appl. Phys. Lett. **107**, 093507 (2015).